Ghost imaging based on the control of light source bandwidth

Zhao-Qi Liu(刘兆骐), Yan-Feng Bai(白艳锋)†, Xuan-Peng-Fan Zou(邹璇彭凡), Li-Yu Zhou(周立宇), Qin Fu(付芹), and Xi-Quan Fu(傅喜泉)‡

College of Computer Science and Electronic Engineering, Hunan University, Changsha 410082, *China*

(Received 28 February 2022; revised manuscript received 3 May 2022; accepted manuscript online 12 May 2022)

A scheme to improve the quality in ghost imaging (GI) by controlling the bandwidth of light source (BCGI) is proposed. The theoretical and numerical results show that the reconstruction result with high quality can be obtained by adjusting the bandwidth range of the light source appropriately, and the selection criterion of the bandwidth is analyzed by the power distribution of the imaging target. A proof-of-principle experiment is implemented to verify the theoretical and numerical results. In addition, the BCGI also presents better anti-noise performance when compared with some popular GI methods.

Keywords: ghost imaging, light source property, spatial frequency domain

PACS: 42.30.Va, 42.30.Kq, 42.50.–p **DOI:** 10.1088/1674-1056/ac6edd

1. Introduction

Ghost imaging (GI) is a nonlocal imaging technology to reconstruct the information of an unknown object by calculating the intensity correlation of two spatially independent beams. The test beam is interacted with the object and is received by the single-pixel detector or a bucket detector. The reference beam is directly measured by a pixel array detector. GI was put into practice in laboratory for the first time by using entangled photon pairs generated by spontaneous parametric down-conversion in 1995.[1,2] Discussions about the properties of the light source had aroused wide attention, which finally reached an accepted conclusion that classical sources can also be used to realize GI.[3–8] Next, many meaningful studies have been carried out to deepen the understanding of GI or improve the imaging quality, such as the light source properties,[9–15] transmission path,[16–20] algorithms of correlation calculation,[21–26] etc.

Transform domain analysis is an important method in the field of signal analysis, and it has been proved that the corresponding methods can be used to improve the performance of GI.[27–34] Jack *et al.* demonstrated the contrast enhancement of images by the use of phase filters in frequency domain.[27] Later, the method based on wavelet trees is presented to reduce the reconstruction time and measurements required for any image size.[28] More recently, Sprigg *et al.* reported an experimental demonstration of a nonclassical imaging mechanism beyond the Rayleigh limit by using spatial-frequency filters.[30] In the same year, a GI scheme with fast Walsh–Hadamard transform is proposed to greatly reduce the reconstruction time.[31] In the above works, transform domain analysis focused on the detection end, which are post-processing methods. In this paper, we firstly propose a scheme to obtain a high quality GI by using the transform domain method on the light source, i.e., the pretreatment method. The numerical and experimental results show that controlling the rang of bandwidth of light source can improve SNR of ghost-image greatly, and show good anti-noise performance especially for the noise from the light source.

2. The model and theory

Ghost imaging system by controlling the bandwidth of light source (BCGI) is shown in Fig. 1. The laser illuminates the spatial light modulator (SLM) controlled by the computer to produce the filtered patterns. The origin of filtered patterns is shown on the left in Fig. 1. A speckle pattern is converted to spatial frequency domain through the Fourier transformation (FT) for low-pass filtering, and then the filtered pattern is obtained by the inverse Fourier transformation (IFT). Then, the modulated light illuminates the object and the light transmitted by the object is received by the bucket detector (BD).

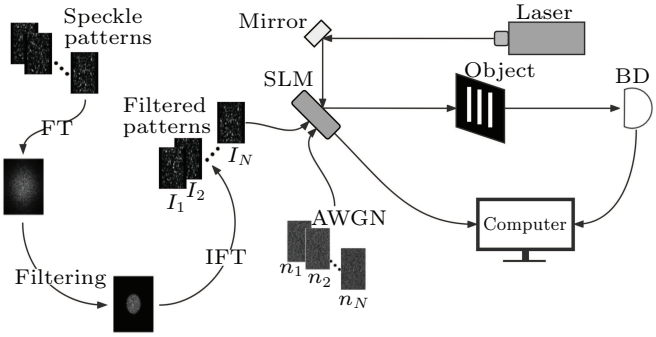


Fig. 1. Scheme of BCGI.

In the framework of conventional GI, the corresponding measurement value B_k from BD for a speckle pattern $I_k(x,y)$

†Corresponding author. E-mail: fybai@hnu.edu.cn
‡Corresponding author. E-mail: fuxq@hnu.edu.cn

© 2023 Chinese Physical Society and IOP Publishing Ltd

can be expressed as[23]

$$B_k = \iint \mathrm{d}x\mathrm{d}y I_k(x,y)T(x,y), \quad (k = 1,2,\ldots,N), \tag{1}$$

where $T(x,y)$ is the transmission function of the object and k represents the number of measurements. The object image O can be retrieved by calculating the intensity correlation between the speckle patterns I and the bucket detector data B, i.e.,

$$O = \langle IB\rangle - \langle I\rangle\langle B\rangle, \tag{2}$$

where $\langle\cdot\rangle$ means the ensemble average.

Compared to the transmission function T, the reconstruction O is often accompanied by a large amount of background noise, which comes from the GI system itself. In general, the noise is evenly distributed across all parts of the frequency domain and it provides the basis for image denoising. In digital image processing, frequency domain filtering based on FT is a simple and effective denoising method. As we all know, the power of an image chiefly concentrates in the lower frequency part, and the power in the medium-high frequency could only supplement the details to the image. Therefore, the noise can be reduced with losing some image's details by low-pass filtering of the data from the detection end. Then, we can put this operation on the front end, i.e., the light source to reduce the hardware requirements. To analyze the possibility, the following operations are implemented.

First of all, the speckle pattern is filtered, which can be expressed as

$$\widetilde{I}_k(x,y) = \iint \mathrm{d}x'\mathrm{d}y' I_k(x',y')h(x-x',y-y'), \tag{3}$$

where $\widetilde{I}_k(x,y)$ represents the filtered patterns, $h(x,y)$ is the convolution kernel used to control the bandwidth of the initial patterns, and it can be obtained from

$$h(x,y) = \begin{cases} 1, & (x^2+y^2) \le r^2, \\ 0, & (x^2+y^2) > r^2, \end{cases} \tag{4}$$

where r represents the filter bandwidth.

Then, the bucket detector data B_k is rewritten as

$$\widetilde{B}_k = \iint \mathrm{d}x\mathrm{d}y \left[\iint \mathrm{d}x'\mathrm{d}y' I_k(x',y')h(x-x',y-y')\right] T(x,y). \tag{5}$$

When $h(x,y)$ satisfies the equation $h(x,y) = h(-x,-y)$, the order of the two integrals in Eq. (5) can be exchanged,[35] and Eq. (5) can be rewritten as

$$\widetilde{B}_k = \iint \mathrm{d}x'\mathrm{d}y' \left[\iint \mathrm{d}x\mathrm{d}y T(x,y)h(x-x',y-y')\right] I_k(x',y'). \tag{6}$$

For a low-pass filter, $h(x,y) = h(-x,-y)$ is obviously satisfied. The reconstruction image O can be directly obtained by low-pass filtering the light source, by which we can acquire some unanticipated benefits. On the one hand, it can be found that when a convolution kernel satisfies some conditions, using the convolution kernel to perform a convolution operation on speckle images is equivalent to performing a corresponding convolution operation on the object's image. On the other hand, our scheme may has unexpected anti-noise performance when compared with directly processing the reconstruction image.

In practical applications, the convolution operation is often time-consuming for Eq. (3). So the filtered patterns can also be calculated by $\widetilde{I} = \mathcal{F}^{-1}[\mathcal{F}(I)\mathcal{F}(h)]$.

3. Results and analysis

In this section, we numerically and experimentally investigate the effect of controlling spatial frequency bandwidth of light source on the imaging quality. The signal-to-noise ratio (SNR, in units of dB) is quoted to quantitatively evaluate the quality of reconstruction images[24]

$$\mathrm{SNR} = \frac{\sum_{i=1}^{m}\sum_{j=1}^{n}\left[T(i,j)-\overline{T}\right]^2}{\sum_{i=1}^{m}\sum_{j=1}^{n}\left[O(i,j)-T(i,j)\right]^2}, \tag{7}$$

where $\overline{T} = \langle T(i,j)\rangle$, $T(i,j)$ and $O(i,j)$ are the transmission matrices of the object mask of size $m\times n$ and the reconstruction image, respectively.

To better show the performance of BCGI, two objects with 128×128 resolution are used in simulations. The one is a triple slit in Fig. 2(a1) and the another one is a binary graphic called blobs consisting of rich points and lines in Fig. 2(c1). Figures 2(a2)–2(a7) represent the reconstruction images in conventional GI, DGI, CSGI, and BCGI with different bandwidth being 0.4, 0.2 and 0.1, respectively. Figure 2(b) represents the corresponding spectrum distributions in Fig. 2(a). By comparing Figs. 2(b1) with 2(b2) and 2(b3), it is found that the frequency domain information of the object is almost submerged in the system noise when traditional GI and DGI are used. While the high frequency noise is effectively removed as CSGI is used, as showed in Fig. 2(b4). After BCGI scheme is used in Figs. 2(b5)–2(b7), the low frequency information of the object is more obvious as the bandwidth decreases. So, imaging quality in CSGI and BCGI is better than conventional GI and DGI. Here, it is noted that there are some overlaps in Fig. 2(a4) although CSGI can obtain a higher SNR for the simple object when compared with BCGI in most cases. Then, for the complex object in Fig. 2(c1), BCGI has better performance than CSGI. As a supplement, a proof-of-principle experiment is implemented to prove the numerical results. A double slit in Fig. 2(e1) is chosen as imaging object, and the corresponding results are shown in Figs. 2(e) and 2(f). Here, the double slit has a slit width 0.8 mm and center-to-center separation 1.4 mm. Obviously, BCGI has better performance than DGI and CSGI, which agrees well with the numerical results. In other words, imaging quality can be improved significantly by choosing appropriate source bandwidth.

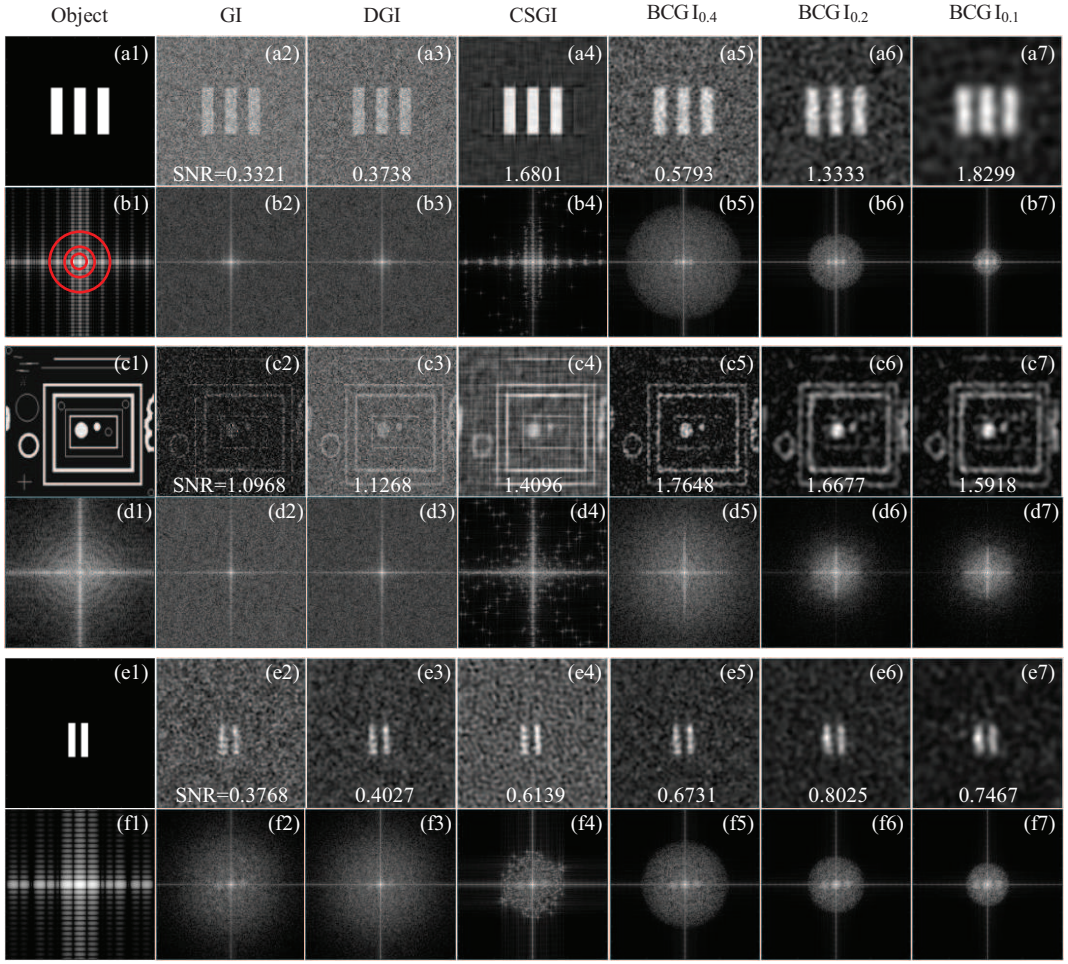


Fig. 2. Simulative and experimental results. (a1) and (c1) The imaging objects of triple slit and blobs for simulations. (a2)–(a7) and (c2)–(c7) Reconstruction images of conventional GI, DGI, CSGI and BCGI at different bandwidths. (b) and (d) The corresponding spectrum distributions of (a) and (c), respectively. (e) and (f) The corresponding experimental results of a double slit (e1). The number of measurements is 5000.

In simulations, note that the SNR increases in Figs. 2(a5)–2(a7) but decreases in Figs. 2(c5)–2(c7). The reason for the difference is that the blobs has more complicated detail information than the triple slit, and the detailed information has lost a lot when the bandwidth being 0.2 or 0.1 so that the quality of retrieved images in Figs. 2(c6) and 2(c7) becomes worse than the one in Fig. 2(c5). To further explain the phenomena shown in Fig. 2, we investigate the power distributions in spatial frequency domain of the three objects when different cut-off frequencies are used. Figure 3 depicts the relationship between the proportion of object power (the ratio of the object power within the specified frequency to the total power) and the normalized cut-off frequency. The square, delta and circle symbols represent the results for the triple slit, blobs and double slit, respectively. It is obvious that the power proportion is proportional to the normalized cut-off frequency and the curve of blobs is relatively smoother than that of the triple slit and double slit. The proportion of object power is 80% for the blobs when the cut-off frequency is between 0.3 and 0.4, which corresponds to better imaging quality, as shown in Fig. 2(c5). So, we can define 80% proportion of the object power as the criteria of choosing the optimal cut-off frequency. Then, we use the criteria to analyze the case of another object. As for the triple slit, the corresponding cut-off frequency is about 0.1 which corresponds to about 80% proportion of object power, and the result is consistent with that in Fig. 2(a7). Moreover, the maximum SNR of experimental results is gained in Fig. 2(e6) when the proportion of object power is about 80%, which is consistent with simulations.

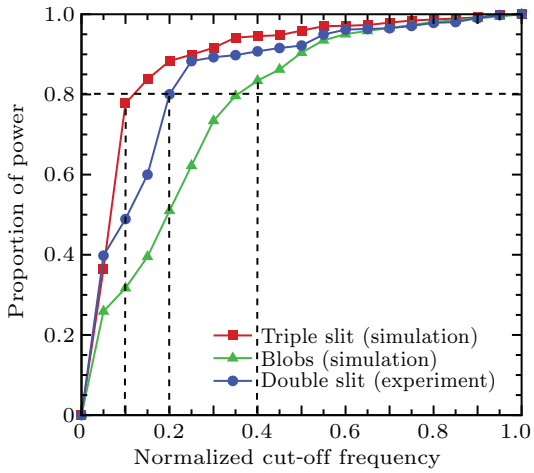


Fig. 3. The power distribution in spatial frequency domain of three target objects under different cut-off frequencies.

Finally, the anti-noise properties of BCGI are analyzed. Here, we add the additive Gaussian white noise with different levels into the light source, and the input signal-to-noise ratio (ISNR, in units of dB) is used to character the noise level. Here, ISNR is defined as[36]

$$\mathrm{ISNR} = \frac{\sum_{i=1}^{m}\sum_{j=1}^{n}|I(i,j)|^2}{\sum_{i=1}^{m}\sum_{j=1}^{n}|N(i,j)|^2}, \tag{8}$$

where I and N represent the signal pattern and noise pattern of size $m \times n$, respectively. At the same time, we choose three popular GI methods for comparison, which are GI, differential GI (DGI),[22] and compressive sensing GI (CSGI).[23] The reconstruction results are shown in Fig. 4. It can be seen that as ISNR decreases, the object information in the reconstruction images of CSGI, DGI and GI is gradually submerged in the noise. While the results in BCGI have almost no changes by comparing the changes of SNR marked in each picture.

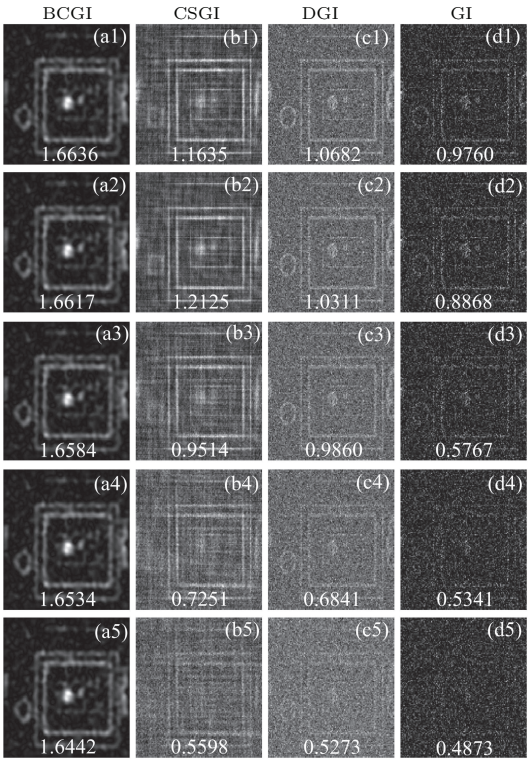


Fig. 4. Simulation results after adding the noise into light source. From the first row to the fifth row, ISNR = 12 dB, 9 dB, 6 dB, 3 dB and 0 dB, respectively. From first column to fourth column, reconstruction images based on $\mathrm{BCGI}_{0.2}$, CSGI, DGI and GI. The SNR is marked at the bottom of each reconstruction image.

4. Conclusion

In conclusion, we have proposed a new GI scheme by controlling the bandwidth of the light source in spatial frequency domain to improve the imaging quality. BCGI with different bandwidths is numerically and experimentally investigated to present better performance, and the results can be explained by the power proportion of the imaging target under different cut-off frequencies. In addition, it is proved that BCGI shows significantly better anti-noise property than CSGI, DGI and conventional GI.

Acknowledgement

Project supported by the National Natural Science Foundation of China (Grant Nos. 61871431, 61971184, and 62001162).

References

[1] Pittman T B, Shih Y H, Strekalov D V and Sergienko A V 1995 *Phys. Rev. A* **52** 3429
[2] Strekalov D V, Sergienko A V, Klyshko D N and Shih Y H 1995 *Phys. Rev. Lett.* **74** 3600
[3] Bennink R S, Bentley S J and Boyd R W 2002 *Phys. Rev. Lett.* **89** 113601
[4] Bennink R S, Bentley S J, Boyd R W and Howell J C 2004 *Phys. Rev. Lett.* **92** 033601
[5] Gatti A, Brambilla E, Bache M and Lugiato L A 2004 *Phys. Rev. Lett.* **93** 093602
[6] Cheng J and Han S S 2004 *Phys. Rev. Lett.* **92** 093903
[7] Cai Y J and Zhu S Y 2004 *Opt. Lett.* **29** 002716
[8] Valencia A, Scarcelli G, D'Angelo M and Shih Y H 2005 *Phys. Rev. Lett.* **94** 063601
[9] Liu H L and Han S S 2008 *Opt. Lett.* **33** 000824
[10] Ferri F, Magatti D, Sala V G and Gatti A 2008 *Appl. Phys. Lett.* **92** 261109
[11] Luo C L and Cheng J 2013 *Opt. Lett.* **38** 005381
[12] Khamoushi S, Nosrati Y and Tavassoli S H 2015 *Opt. Lett.* **40** 003452
[13] Luo C L, Cheng J, Chen A X and Liu Z M 2015 *Opt. Commun.* **352** 155
[14] Zhu X N, Fu X Q, Wang B W, Shi X H and Nan S Q 2018 *Opt. Commun.* **425** 185
[15] Klein Y, Schori A, Dolbnya I, Sawhney K and Shwartz S 2019 *Opt. Express* **27** 003284
[16] Huang X W, Bai Y F and Fu X Q 2017 *IEEE. Photon. J.* **9** 1
[17] Huang X W, Deng Z X, Shi X H, Bai Y F and Fu X Q 2018 *Opt. Express* **26** 004786
[18] Liu X L, Wang F, Zhang M H and Cai Y J 2018 *Appl. Sci.* **8** 1479
[19] Fu Q, Bai Y F, Huang X W, Nan S Q, Xie P Y and Fu X Q 2019 *Photonics. Res.* **7** 001468
[20] Huang X W, Nan S Q, Tan W, Bai Y F and Fu X Q 2020 *Opt. Lett.* **45** 1454
[21] Shapiro J H 2008 *Phys. Rev. A* **78** 061802
[22] Ferri F, Magatti D, Lugiato L A and Gatti A 2010 *Phys. Rev. Lett.* **104** 253603
[23] Katz O, Bromberg Y and Silberberg Y 2009 *Appl. Phys. Lett.* **95** 131110
[24] Li M F, Zhang Y R, Luo K H, Wu L A and Fan H 2013 *Phys. Rev. A* **87** 033813
[25] Bai Y F and Han S S 2007 *Phys. Rev. A* **76** 043828
[26] Sun B Q, Welsh S, Edgar M P, Shapiro J H and Padgett M J 2012 *Opt. Express* **20** 016892
[27] Jack B, Leach J, Romero J, Franke-Arnold S, Ritsch-Marte M, Barnett S and Padgett M 2009 *Phys. Rev. Lett.* **103** 083602
[28] Yu W K, Li M F, Yao X R, Liu X F, Wu L A and Zhai G J 2014 *Opt. Express* **22** 007133
[29] Yamazaki Y and Nomura T 2018 *Appl. Opt.* **57** 009375
[30] Sprigg J, Peng T and Shih Y H 2016 *Sci. Rep.* **6** 38077
[31] Wang L and Zhao S M 2016 *Photonics. Res.* **4** 000240
[32] Chen X H, Kong F P, Fu Q, Meng S Y and Wu L A 2017 *Opt. Lett.* **42** 005290
[33] Guo K X, Bai Y F and Fu X Q 2019 *Opt. Commun.* **444** 120
[34] Zhang W X, Wu Y K, Wu J Z, Liu N, Liu Y X, Liu Z j and Xue P 2021 *Appl. Opt.* **60** 809
[35] Zhou L Y, Huang X W, Fu Q, Zou X P F, Bai Y F and Fu X Q 2021 *Chin. Opt. Lett.* **19** 121101
[36] Wong J W 2013 *Encyclopedia of Radiation Oncology* (Berlin: Springer Berlin Heidelberg) pp. 789–790